View metadata, citation and similar papers at core.ac.uk
brought to you by CORE
provided by NASA Technical Reports Server

N94-35624

OPTIMUM SATELLITE RELAY POSITIONS
WITH APPLICATION TO A TDRS-1 INDIAN OCEAN RELAY

A. H. Jackson
NASA Goddard Space Flight Center
Greenbelt, MD 20771

P. Christopher
Stanford Telecom
Reston, VA 22090

Abstract

An Indian Ocean satellite relay is examined. The relay satellite position is optimized by minimizing the sum of downlink and satellite to satellite link losses. Osculating orbital elements are used for fast intensive orbital computation. Integrated Van Vleck gaseous attenuation and a Crane rain model are used for downlink attenuation. Circular polarization losses on the satellite to satellite link are found dynamically. Space to ground link antenna pointing losses are included as a function of yaw and spacecraft limits. Relay satellite positions between 90 to 100 degrees East are found attractive for further study.

1.0 BACKGROUND

The Tracking and Data Relay Satellite System (TDRSS) has provided vital communication relay service between low altitude satellites and White Sands, New Mexico. Figure 1 shows a polar view of the Earth and relative positions of TDRS East and TDRS West. The ground station at White Sands looks southwest toward TDRS West and southeast to TDRS East. The complementary coverage of western and eastern relays allows nearly full time communication links with low altitude satellites. The complementary coverage is implied by the view of the Earth as seen from TDRS West as shown in Figure 2 and the view from TDRS East (Figure 3). Figures 2 and 3 imply that the Indian Ocean region is a region of concern for marginal communication. Indeed, viewers who watched the Hubble Space Telescope (HST) repair saw excellent video until HST passed over the Indian Ocean. The video flickered and was gone, just that quickly. Approximately four minutes later the link to TDRS West was established as HST approached Malaysia.

We examine the possibility of an Indian Ocean relay to augment TDRSS communication. Figure 4 shows the view from a possible Indian Ocean relay. A ground station in southeastern Australia may be considered for the uplink. The ground station, Tidbinbilla (35.402S, 148.981E), is marginally within view of the relay at 90 degrees East. The ground station would be expected to suffer signal attenuation at low antenna elevation angle. Here we see the first part of a two horned dilemma. The ground station attenuation could be relieved by transferring the Indian Ocean relay eastward to raise the Australian ground station elevation angle. However, this would aggravate the space-space link (SSL) losses in terms of both free space loss and multipath loss. (Multipath loss was related to the video flicker from HST before the signal disappeared). It is difficult to reach a compromise between these competing demands unless the system designer defines some overall system objective function.

Here, we choose a conceptually simple and useful objective function composed of the sum of downlink and SSL losses. We seek to minimize this "Total Loss" objective function to optimize system performance. This concept will apply to any ground station, any relay, and any low altitude user for very general results.

The optimization is computationally intensive. The simulation for the relay must include the SSL link to a low altitude satellite such as the Gamma Ray Observer (GRO) at 5 second intervals. Multipath statistics are compiled for periods of at least 24 hours at each relay position. The intensive computations require efficient, accurate algorithms at every step. We begin by using a method of osculating elements to simulate orbits quickly and accurately for altitudes ranging from 200 to over 42000 km. At each time, a number of losses must also be calculated on both the space to ground link (SGL) and the space-space link (SSL).

The space to ground losses include:

- Gaseous attenuation
  - Water vapor
  - Oxygen
  - Crane rain attenuation
- SGL antenna loss due to limit imposed by antenna stops and yaw
- Free space loss

MIS019B

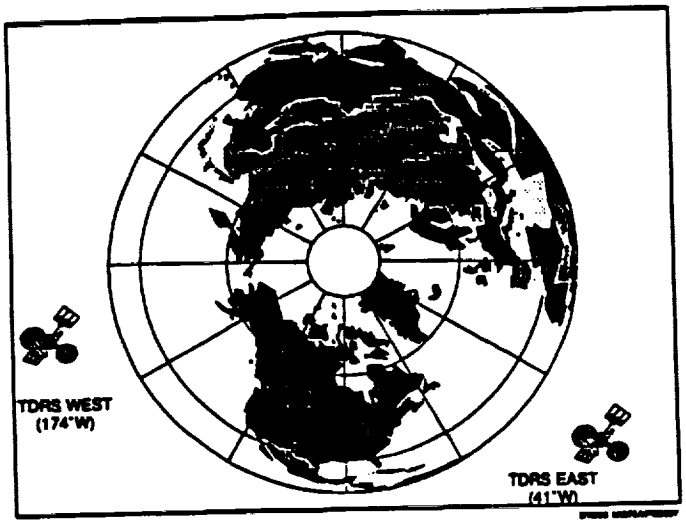

Figure 1: Polar View Showing TDRS Positions at 41°W, 174°W

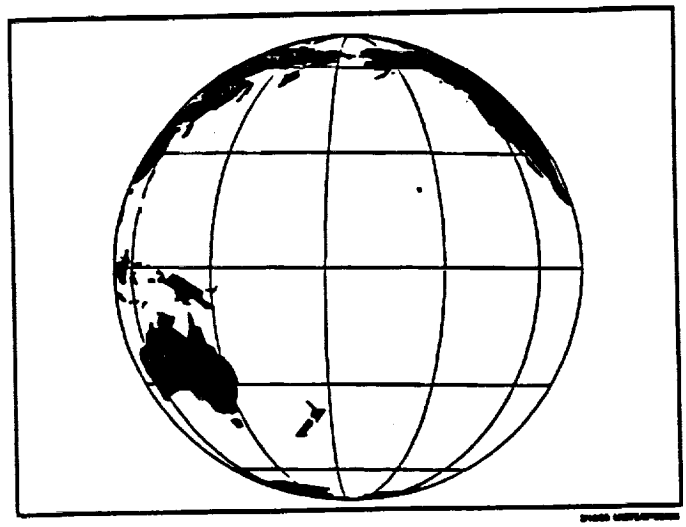

Figure 2: View of Earth from TDRS West (174°W)
Mathematica Orthographic Projection

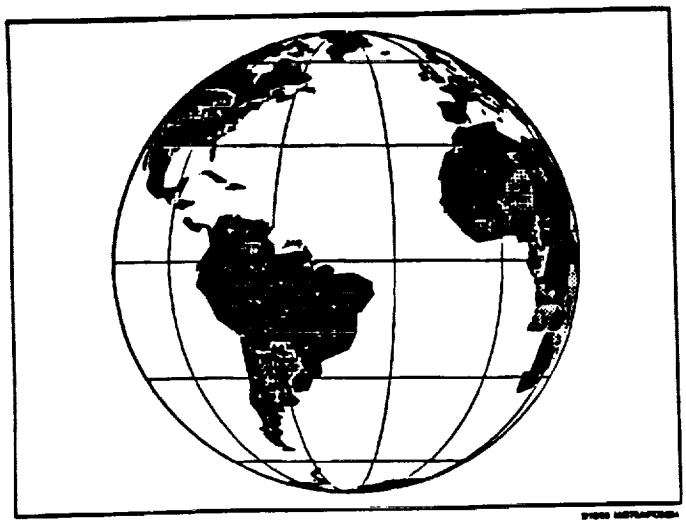

Figure 3: View of Earth from TDRS East (41°W)
Mathematica Orthographic Projection

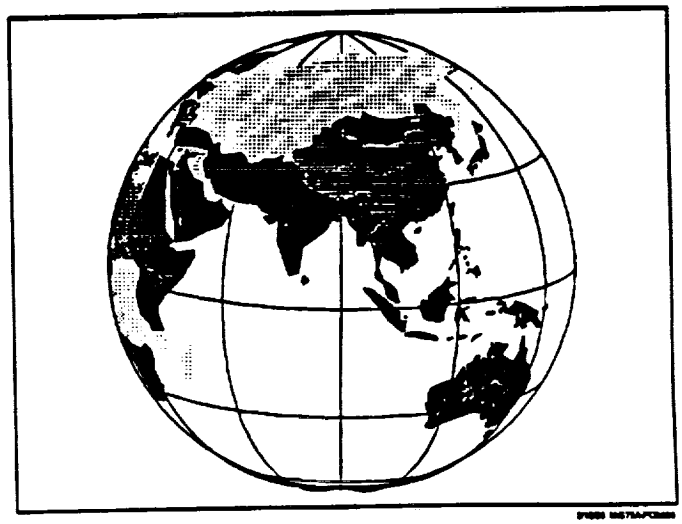

Figure 4: View of Earth from an Indian Ocean Relay at 90°E
Note Southeastern Australia is Barely Visible

MIS019B

SSL losses include:

- Two ray interference for multipath loss
  - Earth grazing ray attenuated by TDRS antenna pattern, gaseous attenuation
- Free space loss

We first show some key results for the method of osculating elements, along with a relatively new and unused result for lunar perturbations. Short expressions for the loss terms follow. Intermediate level results are shown for a relay which has no yaw or SGL antenna restrictions. The paper concludes with three dimensional plots of total loss as a function of longitude and relay yaw for a relay at 8 degree inclination. A TDRS1/GRO example demonstrates the method and indicates practical optimum relay positions.

2.0 ORBITAL ANALYSIS

The method of osculating elements is used here for speed and accuracy in orbital computation. This method has been used by classical astronomers [1]. The method relies on an initial set of Keplerian elements which changes continuously due to a non-central force field. Typical non-central forces to be considered are:

1.	Oblate earth gravitational force	(included here)
2.	Higher earth gravitational force terms	(no available result for osculating elements)
3.	Moon and sun perturbations	(Ash 1974)
4.	Air drag	(omitted here)
5.	Radiation pressure	(omitted here)

The method of osculating elements has often been avoided because it requires analytic derivations for rates of change for the classical orbital elements. Ash [2] has removed some of these objections with a derivation of the smoothed rates of change of orbital elements due to lunar perturbations. Other rates of change were discussed previously in a 1976 SCSC paper [3]. The higher earth gravitational perturbation terms have not yielded short analytic relations, to our knowledge.

2.1 Oblateness Effects. The oblateness effects have been found to give a regression of nodes

$$\dot{W} = -\frac{3}{2a}\sqrt{\frac{\mu}{a}}\ J_2\left(\frac{R}{P_{SL}}\right)^2 \cos(i) \text{ rad/sec} \qquad (2\text{-}1)$$

The argument of perigee changes as

$$W_p = \frac{3}{4a}\sqrt{\frac{\mu}{a}}\ J_2\left(\frac{R}{P_{SL}}\right)^2 (-1+5\cos^2(i)) \text{ rad/sec} \qquad (2\text{-}2)$$

and the mean anomaly changes as

$$M = \frac{3}{4a}\sqrt{\frac{\mu}{a}}\ J_2\left(\frac{R}{P_{SL}}\right)^2 \sqrt{1-e^2}\ (-1+3\cos^2(i)) \text{ rad/sec} \qquad (2\text{-}3)$$

W = right ascension, rad
W_p = argument of perigee, rad
R = earth radius, km

Where μ = earth gravitational constant
$= 0.39860064 * 10^6 \text{ km}^3/\text{sec}^2$
$P_{SL} = a(1-e^2)$ = semilatus rectum
$J_2 = 1.082635 * 10^{-3}$

a = semimajor axis, km
e = eccentricity
i = inclination (deg.)

These are the three main perturbing effects which will concern us as we implement the method of osculating elements. Even these first order effects are interesting. The argument of perigee has a stationary point (at $\cos^2 i = 1/5$, or $i = 63.43°$). This is the basis of a stable "Molniya" satellite communication orbit which has been serving the USSR for over two decades. The stability at $i = 63.43°$ has been a concern for decades, and it is still being studied.

2.2 Lunar Perturbations

In the early 1970's, MIT's Lincoln Lab was concerned with satellites at geosynchronous altitudes and higher. The moon is a leading source of perturbations at geosynchronous altitude. Lincoln Lab had a Planetary Ephemeris Program (PEP) developed in that period which allowed discrete simulations for the 3 body problem (earth-moon-satellite). PEP required exorbitant amounts of computer time, and Lincoln Lab soon realized that a leading orbital dynamicist should examine the problem, in an attempt to get good orbital solutions in a reasonable runtime. M. Ash found that reasonable solutions could be found by spreading the moon into a ring of equivalent lunar mass. His leading terms for the following satellite perturbations were:

$$\Delta W = -2\pi \left(\frac{\mu_m}{\mu}\right)\left(\frac{a}{P_m}\right)^3 \cos(I_m)\left[\frac{3}{4}+\left(\frac{a}{P_m}\right)^2 - \left[\frac{135}{128}+\frac{315}{128}\cos^2(I_m)\right]\right] \quad \text{rad/orbit}$$

$$\Delta e = -\pi\left(\frac{\mu_m}{\mu}\right)\left(\frac{a}{P_m}\right)^3 e\sin(2W_p)\left[-\frac{15}{4}\sin^2(I_m)+ \frac{a^2}{P_m}\left[\frac{315}{128}-\frac{315}{16}\cos^2(I_m)+\frac{2205}{128}\cos^4(I_m)\right]\right] \quad \text{rad/orbit}$$

$$\Delta W_p = \pi\left(\frac{\mu_m}{\mu}\right)\left(\frac{a}{P_m}\right)^3\left[3-\frac{15}{2}\sin^2(W_p)\sin^2(I_m)\right]+\frac{a^2}{P_m} \text{ (continued)}$$

$$\left[-\frac{45}{32}+\frac{315}{64}\sin^2(W_p)+\left(\frac{225}{32}-\frac{315}{8}\sin^2(W_p)\right)\cos^2(I_m)\right] \quad \text{rad/orbit}$$

$$\text{Where } \left(\frac{\mu_m}{\mu}\right) = \frac{\text{lunar gravitational constant}}{\text{earth gravitational constant}} = 0.012288$$

I_m = inclination with respect to lunar plane
P_m = mean lunar distance = $3.844 \cdot 10^5$ km from geocenter

This spreading of lunar mass into an equivalent thin lunar annulus allowed these relatively short, computationally efficient equations. However, actual runs of the PEP revealed a difference in stability between prograde and retrograde satellite orbits. The difference in stability was traced to unstable semimajor axis and eccentricity. Figure 5 shows retrograde orbits as more stable than posigrade.

2.3 Comparison of Prediction Methods

Numerical integration techniques may be broadly compared to the method of osculating orbital elements as in Figure 6. The first two numerical integration methods are found in NASA SP-33 [4,5]. The last entry, for osculating orbital elements, is our own addition to the table. The osculating elements offer a good speed comparison, but a different kind of error is seen. A particular 8 hour orbit may resonate as a harmonic of the Earth's third order gravitational potential, and grievous error may result from this latter method.

In practice, the method of osculating elements has shown good accuracy for TDRS and all users with altitude greater than 200 km.

3.0 PROPAGATION EFFECTS

The signal loss on the space-to-space link (SSL) and the attenuation losses at Tidbinbilla are interesting in their own right. The SSL losses are seen to increase as the relay shifts eastward, and the ground station losses to increase as the relay shifts westward. They must be studied in detail in order to minimize the sum of losses by shifting the longitude of the Indian Ocean relay.

3.1 Multipath for an Earth Grazing Ray

The space-to-space link between TDRS and the user may be degraded by a variety of mechanisms. Figure 7 shows the signal degradation mechanisms which we consider here. The ray tangent height (HGRAZ) is a key influence on multipath interference. Two ray multipath interference is the dominant effect. The reflected ray is considered as a specular reflection which interferes with the direct ray. Three ray interference models have been shown by Rummler to give good comparisons to actual multipath conditions, but we use only two rays here for simplicity and for maximum constructive and destructive interference. Minimum signal results when the reflected ray is 180 degrees out of phase with the direct ray. These effects would be severe for linearly polarized rays, with large variations in received signal amplitude for the TDRS-user link. Horizontal polarization gives deeper signal fades than vertical polarization. Fortunately, the TDRSS SSLs have avoided these deep fading possibilities by using circular polarization.

Circularly polarized links, such as the TDRSS SSLs, have more benign fading than linear polarization. H. R. Reed [6] has shown the vector sum of the direct and interfering circularly polarized rays. His general analysis concludes with:

$$\frac{E_R}{E_o} = \left[1+\left(\frac{D}{2}\frac{E_r'}{E_o}\right)^2 + 2D\left(\frac{E_r'}{2E_o}\right)\cos(\theta-\phi_h+\alpha)\right]^{1/2} \quad (3\text{-}1)$$

MIS019B

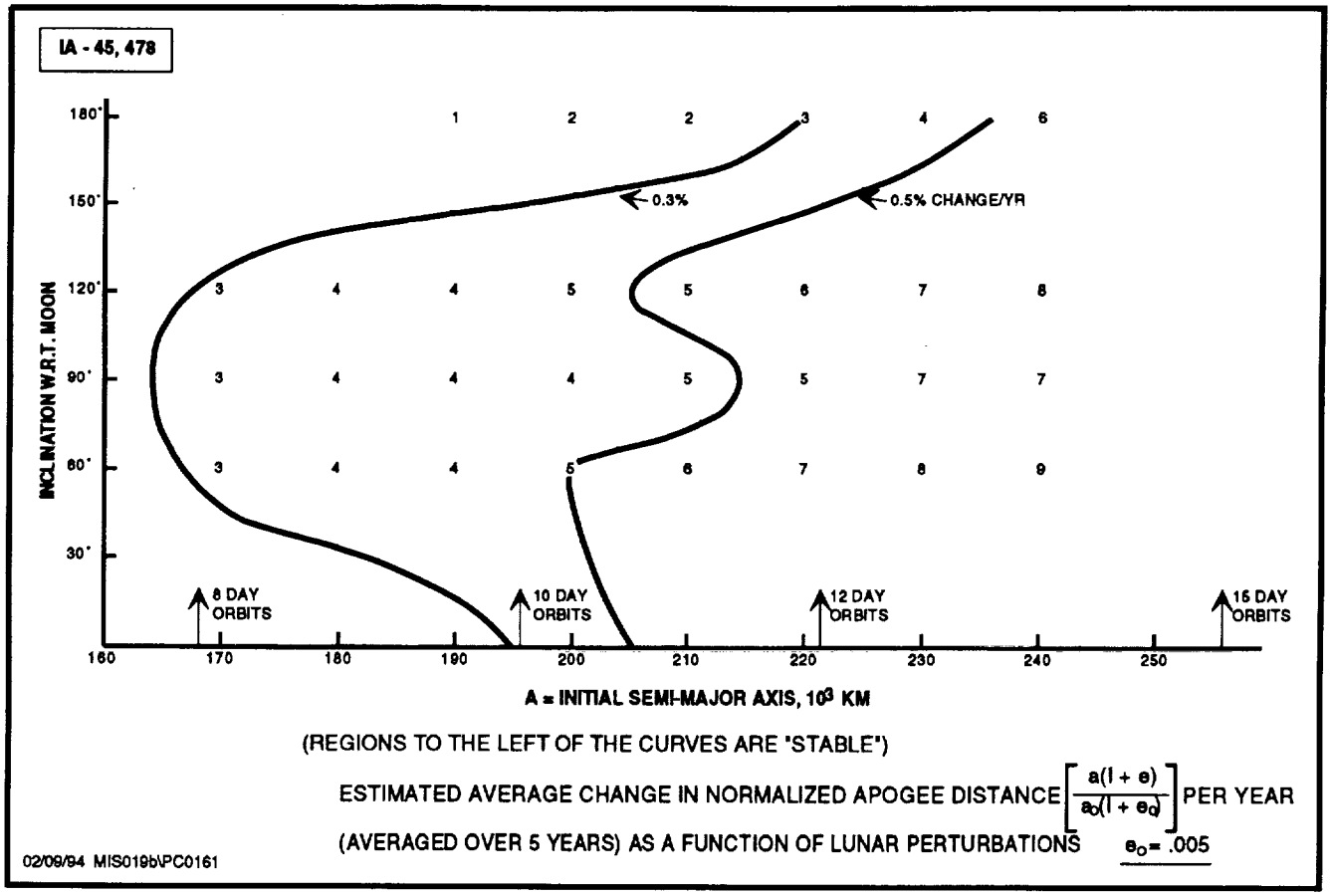

Figure 5: Instability Regions Due to Lunar Perturbations

Method	Ease of Changing Step Size	Speed	Stability	Error
Runge-Kutta Numerical Integration	*	Slow	Stable	Satisfactory Roundoff
Bowie Numerical Integration	Easy	Fast	Stable	Satisfactory Roundoff
Method of Osculating Elements	Easy	Very Fast	Stable	**

* Difficult to determine proper step size.

** No roundoff error, but missing higher order earth gravitational terms (usually unimportant unless orbit is a harmonic of a third order perturbation, as for an 8 hour inclined orbit).

Figure 6: Short Comparison of Prediction Methods

MIS019B

and

$$E_r' = E_o\left[R_v^2 + R_h^2 + 2R_vR_h\cos(\phi_h - \phi_v)\right]^{1/2} \text{ volts/meter} \quad (3\text{-}2)$$

where

E_R = received voltage amplitude

E_o = received voltage amplitude in absence of reflection

D = divergence factor

E_R' = received reflection voltage amplitude

α = additional phase lag, rad. = 0

θ = path lag of reflected wave, rad

ϕ_h = reflection phase lag of horizontal component, rad

ϕ_v = reflection phase lag of vertical component, rad

R_h = magnitude of horizontal reflection coefficient

R_v = magnitude of vertical reflection coefficient.

For low reflection angles, ϕ_h is assumed equal to π rad and ϕ_v equal to zero for this simplified analysis. In addition D is assumed as unity. With these simplifications and the introduction of a front-to-side power ratio (F) (3-2) reduces to:

$$E_r' = \frac{E_o}{\sqrt{F}}\left[-R_v + R_h\right] \quad (3\text{-}3)$$

The front-to-side power ratio consists of both antenna gain and atmospheric attenuation terms.

(3-2) may be substituted into (3-1) to yield:

$$\frac{E_R}{E_o} = \left[1 + \left(\frac{1}{2\sqrt{F}}\right)^2\left[R_h - R_v\right]^2 + \frac{\left[R_h - R_v\right]}{\sqrt{F}}\cos(\theta - \pi)\right]^{1/2} \quad (3\text{-}4)$$

At a given front-to-side ratio (F) and reflection coefficients, $\left(\frac{E_R}{E_o}\right)^2$ is seen to follow the same distribution as a uniformly distributed cosine.

Reed and Russell's result is a good start in describing the received signal amplitude. However, other important signal degradation occurs on the TDRS link, too. Many interesting phenomena occur in the upper atmosphere, as elucidated by a recent IEEE Transactions [7]. This key issue on astronomy and remote sensing has outlined the atmospheric constituents that have been measured at millimeter wavelengths. These include ozone, chlorine monoxide, water vapor, nitrous oxide (N20), HO2, and carbon monoxide in the stratosphere. Measurements in the troposphere (altitudes less than 10 km) have concentrated on water vapor at 22.2 GHz and oxygen transitions at 60 GHz. The primary measurement objectives for future missions, as given by Joe Waters, are shown in Figure 8. Note the entire range of objectives extends to 80 km altitude. We treat only oxygen and water vapor attenuation here, and ray tangent heights less than 50 km will usually be required for noticeable attenuation (multipath fading is another matter, and S-band multipath may occur for ray tangent heights of hundreds of km).

The amplitude of the direct ray suffers attenuation in the upper parts of the atmosphere and the reflected ray is attenuated even more than the direct ray. The reflected ray suffers integrated Van Vleck gaseous attenuation as found in earlier papers [8,9].

$$A_{o_2} = \frac{.34}{\lambda^2}\left(\frac{-H_o}{\sin E}\right)\left[\frac{1}{2K_1}\ln\left(\frac{(\frac{1}{\lambda})^2}{(\frac{1}{\lambda})^2 + K_1v_1^2}\right) + \frac{1}{2K_2}\ln\left(\frac{(2+\frac{1}{\lambda})^2}{v_1^2K_2^2 + (2+\frac{1}{\lambda})^2}\right) + \frac{1}{2K_2}\ln\left(\frac{(2-\frac{1}{\lambda})^2}{(2-\frac{1}{\lambda})^2 + K_2^2v_1^2}\right)\right] \quad (3\text{-}5)$$

dB, total oxygen attenuation (1 GHz < f < 50 GHz)

where K_1 = 0.018

K_2 = 0.049

λ = wavelength in cm

E = elevation angle, radians

MIS019B

Ho = 7 km (oxygen scale height)

v_1 = $\exp(-h_1/H_0)$

h_1 = height of ground reflection point above sea level, km

$$A_{H_2O} = \left(\frac{0.0035}{\lambda^2}\right)\frac{\rho_o}{K_3}\left(\frac{H_o}{SinE}\right)\left[+\frac{2v_1^3}{3} - \frac{a_1}{K_3^2}\left[v_1 - \frac{\sqrt{a_1}}{K_3}\tan^{-1}\frac{K_3 v_1}{\sqrt{a_1}}\right]\right.$$
$$\left. - \frac{a_2}{K_3^2}\left[v_1 - \frac{\sqrt{a_2}}{K_3}\tan^{-1}\left(\frac{K_3 v_1}{\sqrt{a_2}}\right)\right]\right] \quad (3\text{-}6)$$

dB H_2O attenuation.

where K_3 = 0.087,

ρ_o = water vapor density at the earth's surface, g/m^3.

$$a_1 = \left(\frac{1}{\lambda} - \frac{1}{1.35}\right)^2; \quad a_2 = \left(\frac{1}{\lambda} + \frac{1}{1.35}\right)^2$$

The total gaseous attenuation will be assumed to be the sum of Equations 3-5 and 3-6.

Crane's rain attenuation [10,11,12] may also be introduced for earth grazing ray attenuation. It is usually omitted because it is representative of rays less than 4 km altitude.

The TDRS antenna pattern is the final item considered here. The general antenna pattern given by Silver for a uniformly illuminated parabolic dish has been found useful in previous TDRS interference studies [13]. The antenna off-boresight loss for the reflected ray may then be described by:

$$G(U) = 10\log_{10}\left[2\frac{J_1(U)}{U}\right]^2 \text{ dB} \quad (3\text{-}7)$$

where $U = \frac{\pi D}{\lambda}\sin$ (off-boresight angle)

D = antenna diameter, same units as wavelength λ

Equation (4-7) has been found to be useful at the TDRS S, Ku, and Ka-bands.

With

Aa = Gain loss for reflected ray (off-boresight), dB (Equation 3-7).

Aatm = Atmospheric loss for reflected ray - Atmospheric loss for direct ray, dB (Equation 3-5 plus Equation 3-6).

The front-to-side ratio can be found from

$$F_s = 10^{+\left[\frac{(Aa + Aatm)}{10}\right]} \quad (3\text{-}8)$$

and substituted into Equation 3-4 for the magnitude of the received signal amplitude.

Figure 9 shows potential multipath regions in the polar regions. In addition, Reed and Russell show considerable multipath effects within the satellite horizon. We also consider these effects in the results section.

3.2 Ground Station Attenuation

The integrated gaseous attenuation equations of Section 3.1 may also be used for the ground station at Tidbinbilla. The appropriate substitutions are made for ground station elevation angle and ground station altitude above sea level. The rain model proposed by R. K. Crane is used here in the following form:

$$A_R = \frac{H_R}{Sin(E)}\,\alpha_1\,\gamma\,\beta\,R_P^{(\beta-de)} \text{ dB} \quad (3\text{-}9)$$

where:

H_R = Rain model height above ground station, km

E = elevation angle of ground antenna, degrees

$$\alpha_1 = 0.01\left(\frac{F_G}{10}\right)^{2.3502}$$

F_G = Frequency, GHz

$\gamma = 2.3\log_{10}[v]$

MIS019B

$$\nu = H_R/(\tan(e))$$

$$\beta = 1.18 - 0.00475\,(F-10)$$

$$de = 0.3\,\log_{10}[\nu]$$

The height of the model rain cell is typically more than 3 km and is a function of ground station latitude. Dr. Ippolito of Stanford Telecom has pointed out that rain cell height is a function of intensity.

Rain attenuation is intrinsically a probabilistic phenomenon. It has been the subject of many excellent theoretical studies over several decades. Lin [14] has described rain attenuation as lognormal over several orders of magnitude. Our primary interest here is only in the two orders of magnitude between 0.01 and 0.0001 rainfall probability, and a much simpler function is adequate for us.

Rain attenuation may often be treated as a two-parameter exponential probability density function over two orders of magnitude. This is apparent in a form of the Rice Holmberg relations for attenuation given by Dutton [15], and the exponential function has been useful in other derivations. For example, constant elevation angle experiments conducted with Applications Technology Satellite-6 (ATS-6) were quantitatively different at each ground location, but they would be represented approximately by:

$$P\,(A_R \geq A) = \phi \exp - \frac{(A - \lambda)}{\beta}, \text{ for } A \geq \lambda \qquad (3\text{-}10)$$

where rain attenuation $A_R \geq$ an arbitrary attenuation A, dB.

ϕ = fraction of time noticeable rain or cloud attenuation occurs, typically A dB.

λ = lower cut-off for exponential distribution, dB.

β = standard deviation of exponential distribution, dB.

We assume that λ and β can be weighted by (cosecant elevation) so that equation (3-9) can apply to other elevation angles. We also assume that attenuation has a frequency dependence described by Crane's rain model.

A rain region F is assumed for Tidbinbilla. (This will be subject to change). The rain rate at 0.99 exceedance probability is 1.7 min/hr and the corresponding rain rate at the 0.999 level is 5.5 min/hr.

The total atmospheric attenuation (rain attenuation + gaseous attenuation) at Tidbinbilla is seen on Figure 10 to be a strong function of elevation angle. If ground station attenuation were the only concern, the Indian Ocean relay would be located near Australia. However, this would cause multipath losses on the space-space link to increase sharply.

Overall relay communication performance is more closely related to the sum of ground station losses and SSL losses then to any single loss.

4.0 GEOSTATIONARY RESULTS

All three relay satellites are geostationary for these examples. This rare event would occur when TDRS East, TDRS West, and the Indian Ocean relay have 42164 km semimajor axis, zero inclination, and zero eccentricity. The elevation angle from Tidbinbilla to the Indian Ocean relay is therefore constant once the Indian Ocean longitude is chosen. The SSL link to a low orbiter is simulated at 5 second intervals. All three relays are checked for visibility and multipath loss, and the relay which is visible and has minimum loss is chosen as the preferred relay. The minimum loss is saved from interval to interval, and loss statistics are compiled. After 24 hours of orbital simulation, the maximum (of the minimum losses) is added to the uplink loss and saved as SUMLOSS.

Figure 11 shows SUMLOSS results for a range of Indian Ocean relay longitudes. The Gamma Ray Observatory (GRO) is chosen both for its important mission and for its characteristic orbital elements. The GRO semimajor axis is approximately 6829 km and has 28.5 deg. orbital inclination. The downlink losses at 99.9 percentile level are used for the top curve SUMLOSS999. The top curve clearly favors relay positions east of 95 east for S-band SSLs. An absolute minimum is reached in the vicinity of 125 East. The downlink loss is indicated by SGL999 and the average space-space loss is shown as AVSSL. Figure 12 shows conceptually similar results, but for a Ku band SSL. The average SSL loss is lower than the corresponding loss at S band, but the optimum relay position is in the same 125 East vicinity as the S band case.

MIS019B

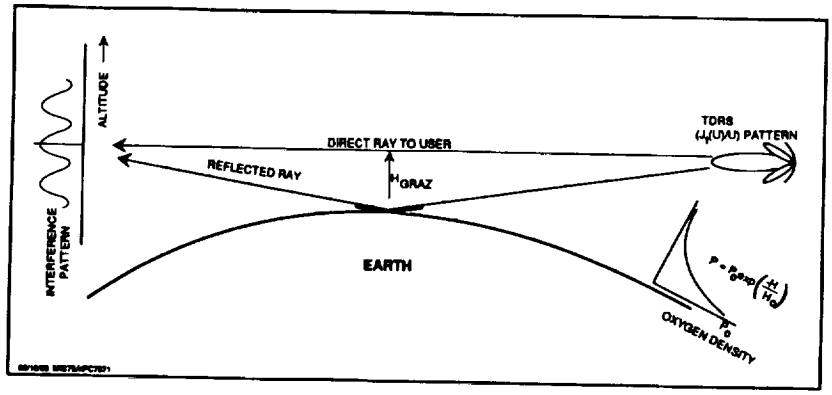

Figure 7: Interference Pattern (Multipath) for a Marginal TDRS - User Link

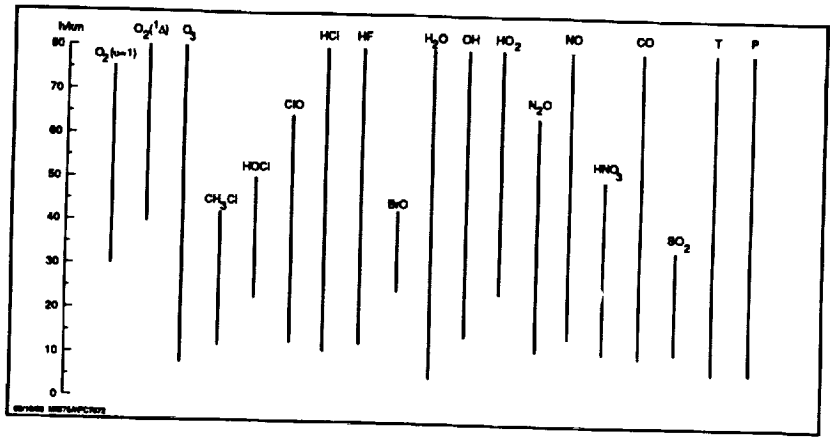

Figure 8: Measurement Objectives for Future NASA Millimeter/Submillimeter Wave Earth Observations (Joe W. Waters, 1992)

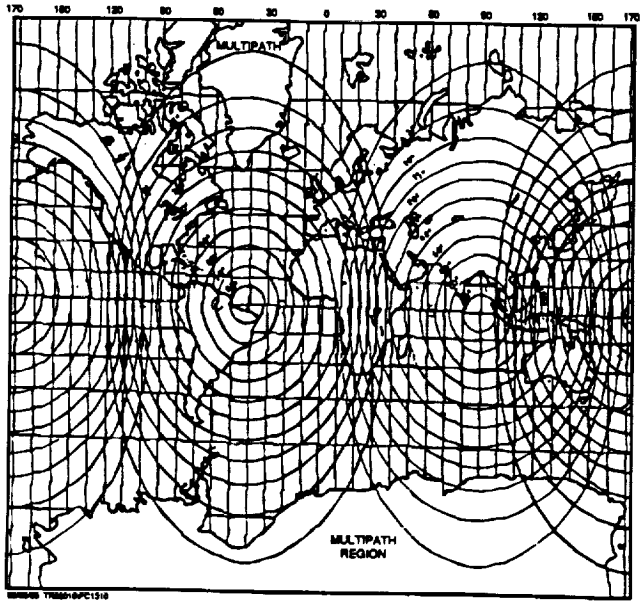

Figure 9: Potential Multipath Regions TDRS at 188° E, 315° E and 90° E

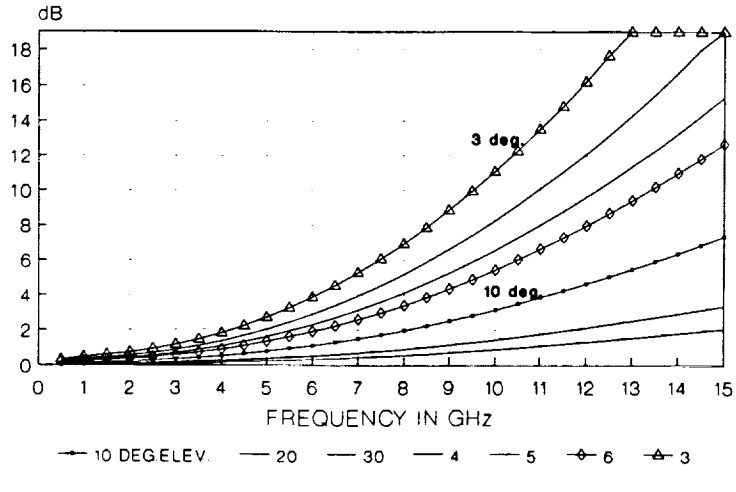

Figure 10: Tidbinbilla Atmospheric Attenuation P=0.999, Region F, Rain Rate=5.5 MM/HR

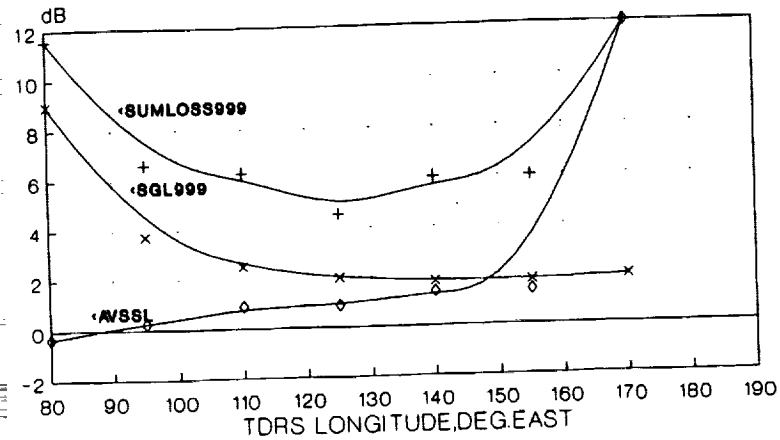

Figure 11: Tidbinbilla-TDRS-GRO Sumloss 2.2875 GHz SSL I_{TDRS}=0

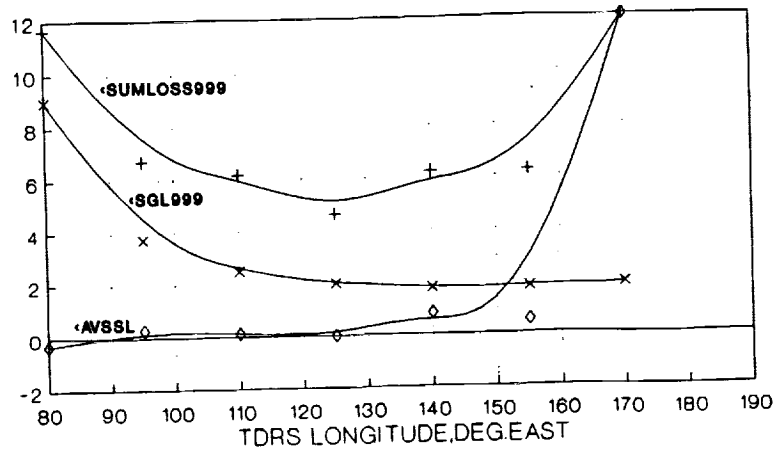

Figure 12: Tidbinbilla-TDRS-15 GHz SSL I_{TDRS}=0

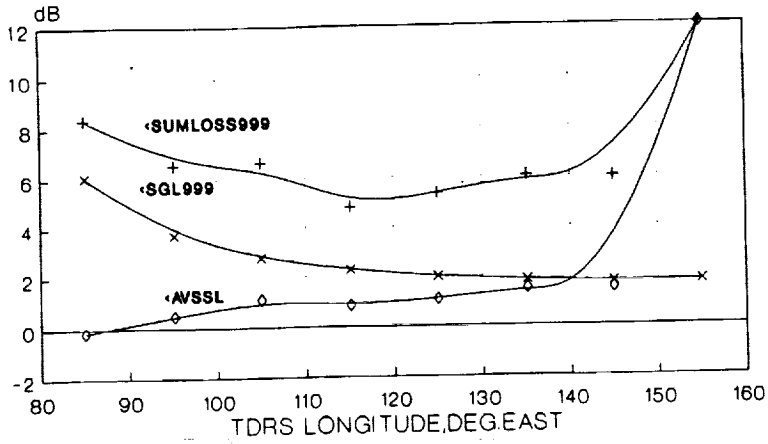

Figure 13: Tidbinbilla-TDRS-Shuttle Sumloss 2.2875 GHz SSL I_{TDRS}=0

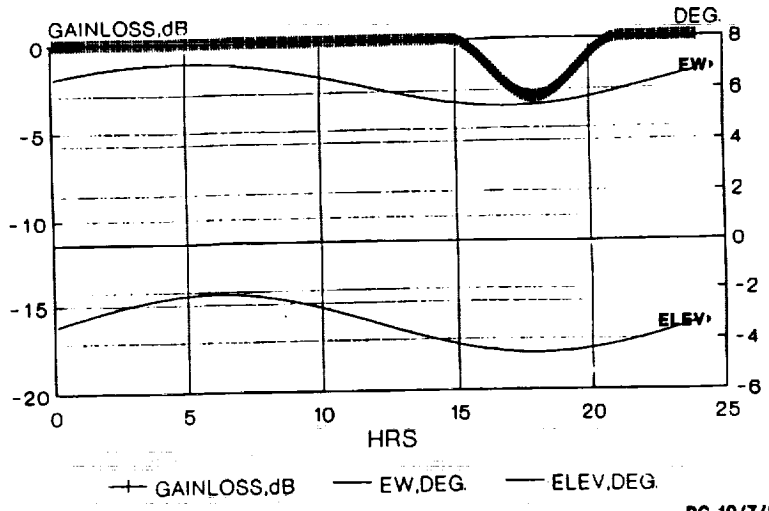

WORST GAINLOSS=-3.26dB
MIN ELEV=-4.539DEG.

PC 10/7/9
A88

Figure 14: 85E to Tidbinbilla I=10 Deg Roll=-2, Yaw=-1.0 Deg, SW2 Limit=-4.155 Deg SGL BW=0.7 Deg F=13.73 GHz

MIS019B

Figure 13 shows results for links to a 200 km altitude satellite, such as the shuttle. The inclination is again 28.5 deg. The optimum relay position is near 115 East for both S band SSL and Ku band SSL.

5.0 TOTAL LOSS FOR NON-GEOSTATIONARY RELAYS

TDRS-1 may have some difficulty in pointing the space to ground (SGL) link antenna toward Tidbinbilla. The antenna is software limited at 4.15 deg. South, and some conditions may require more southerly pointing. Figure 14 shows the diurnal gainloss effects due to mispointing the SGL antenna. The SGL elevation angle is seen to dip below -4.15 deg. elevation (right scale) at 16 hours and the resultant SGL antenna gain (top curve) suffers. Over 3 dB gain loss would be expected in this case. This "worst gain loss" is actually a function of relay longitude, inclination, roll and yaw.

The NASA Flight Dynamics Facility has supplied long term calculations for TDRS-1 inclination. They may be approximated by an equation as [16]

$$i = 4.79178 + 0.393246\,x + 0.128427\,x^2 - 0.0209437\,x^3 + 0.00133576\,x^4 + 0.0000383016\,x^5 + 4.04173\,10^{-7}\,x^6 \text{ deg.}$$

where i = inclination, deg.
X = year after 1990

The inclination may be plotted as Figure 15.

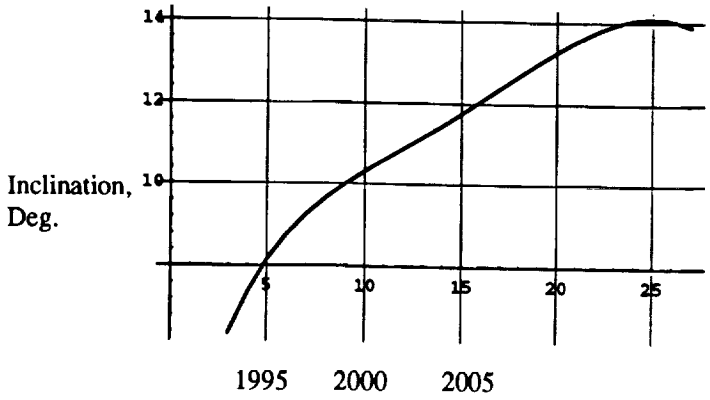

Figure 15 : TDRS-1 Inclination vs. Time

Figure 15 implies an 8 degree inclination in late 1994. An 8 deg. inclination and negative 1.8 deg. roll may be used to examine alternative relay positions. A large array of runs conceptually similar to Figure 14 may be used to generate the gain loss results of Figure 16. The Mathematica two dimensional curve fit for gain loss yields

SGL Gain Loss=
$5.63641\,10^{-6} + 0.000204767\,LON + 0.00450539\,LON^2 - 0.000185253\,LON^3 + 2.61605\,10^{-6}\,LON^4 - 1.4523\,10^{-8}\,LON^5 + 2.77005\,10^{-11}\,LON^6 + 3.63655\,10^{-8}\,Y - 3.56642\,10^{-6}\,LON\,Y - 0.000547018\,LON^2\,Y + 3.43689\,10^{-6}\,LON^3\,Y + 0.000166314\,Y^2 + 0.00910266\,LON\,Y^2 - 0.0000636192\,LON^2\,Y^2 + 7.02275\,10^{-6}\,Y^3 + 0.00079983\,LON\,Y^3 + 0.000391586\,Y^4 + 0.0000232073\,Y^5$

where LON = relay longitude deg.
and Y = YAW, deg.

Figure 16 is difficult to examine quantitatively. Figure 17 shows 1.0 dB contour intervals for a wide range of longitudes and spacecraft yaw. Less than 4.0 dB SGL gain loss is seen for most yaw conditions at relay positions west of 90E.

This provides an interesting contrast for the loss results of Figure 11. The sum of downlink and forward link losses increased sharply for relay positions west of 90E. The sum of uplink losses, forward losses, and SGL gain loss may be shown as total loss in Figure 18, or the Mathematica functional approximation for total loss as

Total Loss=
$0.000301945 + 0.0109703\,LON + 0.241427\,LON^2 - 0.00795836\,LON^3 + 0.0000979854\,LON^4 - 5.32179\,10^{-7}\,LON^5 + 1.07592\,10^{-9}\,LON^6 + 3.61795\,10^{-8}\,Y - 3.57324\,10^{-6}\,LON\,Y - 0.00547041\,LON^2\,Y + 3.43711\,10^{-6}\,LON^3\,Y + 0.000340661\,Y^2 + 0.0092383\,LON\,Y^2 - 0.0000647599\,LON^2\,Y^2 + 7.01938\,10^{-6}\,Y^3 + 0.000799475\,LON\,Y^3 + 0.000566351\,Y^4 + 0.0000231966\,Y^5$

Figure 19 is a contour plot of Figure 18 with 1 dB intervals. A near-minimum total loss condition exists between 98-105 E. The contour plot shows the interesting case of optimum position shifting to 102E for perfect spacecraft attitude control and zero yaw.

Figure 20 allows a closer look at the optimum longitude regions. Finer increments were chosen for the runs, and the entire 90°-100° E region is attractive. It also shows the interesting shift westward for negative yaw.

MIS019B

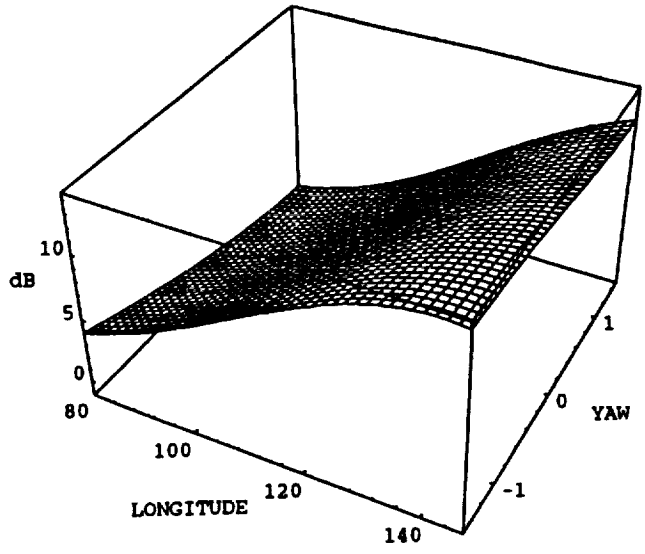

Figure 16: Maximum Gain Loss (dB) as a Function of Longitude and Spacecraft Yaw I = 8°, November 1994

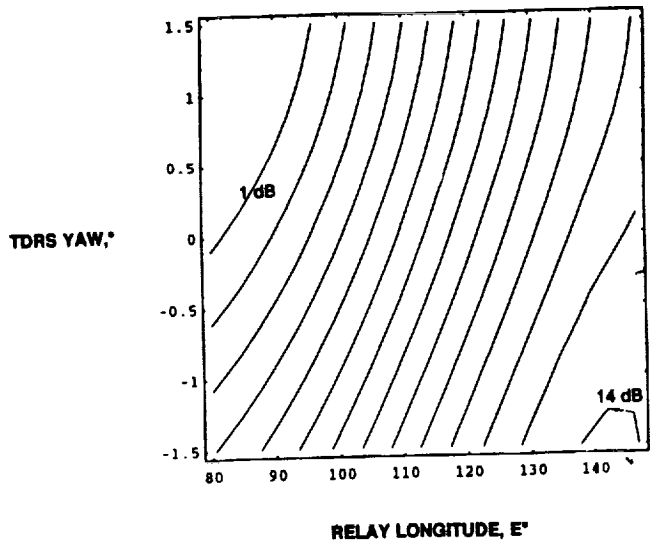

Figure 17: SGL Maximum Gain Loss at 1.0 dB Intervals I = 8°, November 1994

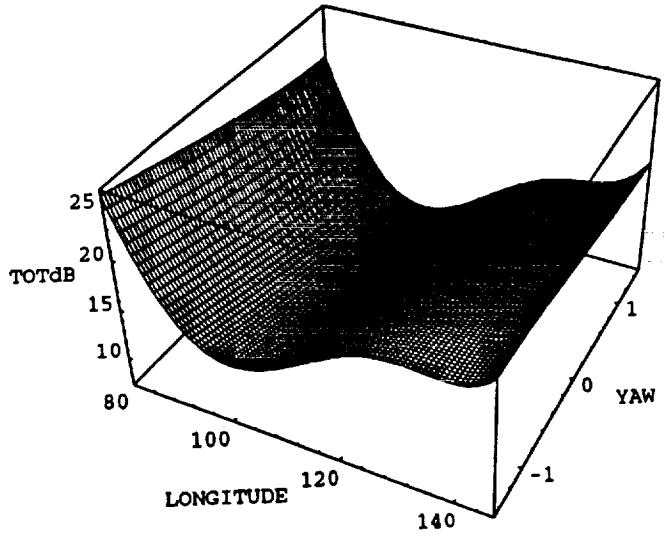

MIS019B

Figure 18: Total Loss as a Function of Longitude and Yaw I = 8°, November 1994

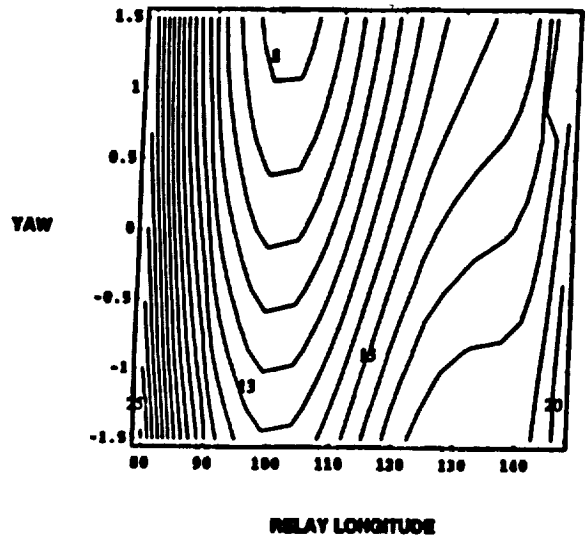

Figure 19: Total Loss at 1 dB Intervals

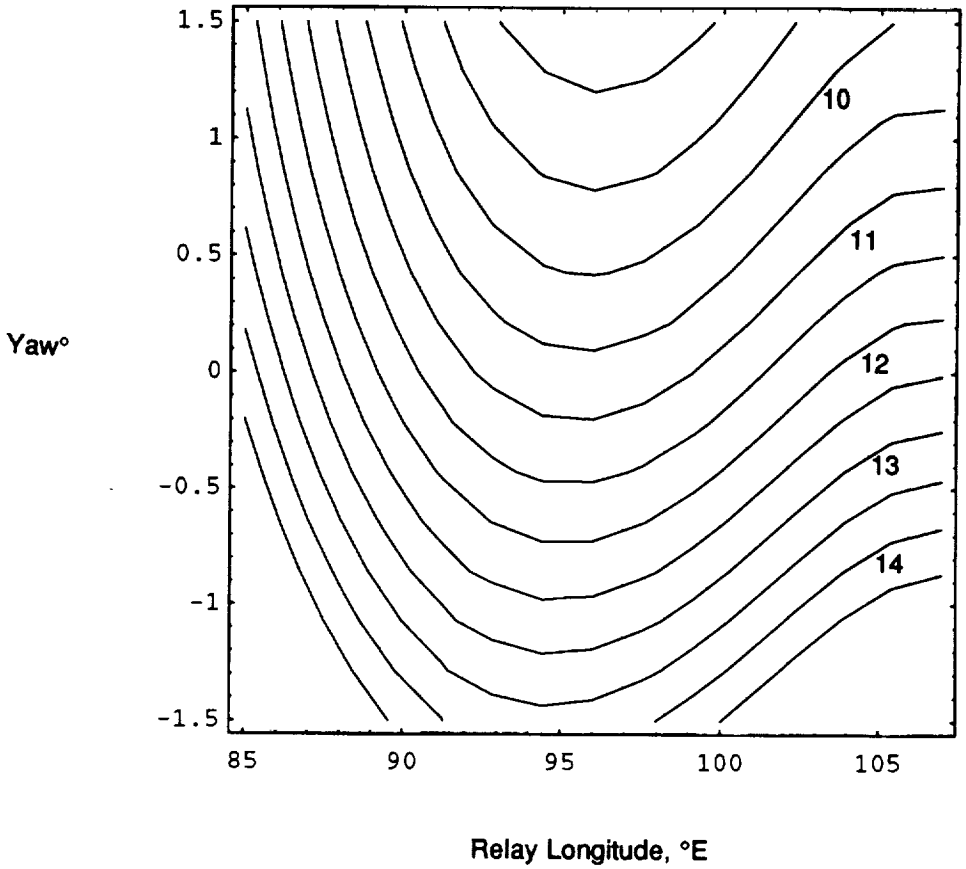

Figure 20: Details of Optimum Relay Region, with Total Loss at 0.5 dB Intervals I=8°, November 1994

MIS019B

The benefits of optimizing TDRS-1 mean longitude continue to grow throughout the decade. Inclination will continue to grow with time (Figure 15), and the Tidbinbilla elevation angle would be expected to drop below 6 degrees for a relay mean longitude of 85°E in August 1998 at an inclination of 10 degrees. This would imply a large gaseous and ran attenuation at the ground station. Relay positions in the 90-100°E region would have sizeable advantages in total loss, as shown in the figures of the Appendix.

6.0 CONCLUSIONS

We have discussed a way to optimize relay satellite positions. The conflicting requirements of good downlinks and good satellite to satellite links were reconciled by minimizing the sum of link losses. This method clearly discriminated against any relay position which offered excessive loss, whether as a low elevation angle at a ground station or as an Earth grazing ray on the relay to satellite link.

The method required fast, accurate orbital computation and concise equations for signal loss on the downlink and the SSL. The method of osculating elements was used to calculate all satellite positions at 5 second intervals for a day at each relay longitude. The analytic rates of change of Keplerian elements were shown in succinct form. The oblate Earth perturbations were very important for low orbiting satellites and Ash's lunar perturbation terms became important at geosynchronous altitude and above.

Gaseous attenuation on both the SSL and the downlink was represented by integrated Van Vleck attenuation for oxygen and water vapor. The downlink also included rain attenuation, as modeled by R.K. Crane. The downlink attenuation typically became excessive at low ground elevation angles. Two ray multipath interference was included on the SSL. The SSL fading became excessive for Earth grazing rays. A special space to ground antenna pointing loss was modeled as a function of roll, pitch, and yaw with the aid of the Euler Theorem and experimental TDRS SGL gain patterns.

The utility of the method was shown with examples of TDRS-1 as an Indian Ocean relay. Optimum TDRS longitudes were seen to be dependent on the orbit of the low altitude satellite user, the SSL frequency, the ground station climate, and the TDRS roll and yaw. TDRS-1 longitudes between 90-100E were seen to be attractive for further study.

The method will be useful for a number of other cases. A variety of downlink and SSL conditions apply not only to future TDRSS concepts, but also to new low altitude satellite communication concepts. Ground stations at a variety of locations may be considered by changing the rain region and coordinates. Space-space link frequencies between 1-55 GHz may be used with the current set of integrated Van Vleck attenuation equations.

Acknowledgements

Shannan Bloomquist solved the Gordian Knot of long equations in narrow columns. George McKay suggested key ways to simplify the figures. Charlo Mullen offered invaluable tips on the legibility of reduced text. Charles Downs of BFEC provided checks on TDRS-1 orbital elements.

REFERENCES

1. Moulton, F. R. (1914). *An Introduction to Celestial Mechanics*, MacMillan Co., N.Y., 1914.

2. Ash, M. (1974). "Doubly Averaged Effect of the Moon and Sun on a High Altitude Earth Satellite Orbit," TN 1974-5, Lincoln Laboratory, 1 March, 1974.

3. Christopher, P., S. M. Maciorowski, and L. Allen (1976). "High Altitude Satellite Communication, with Crosslinks." Proceedings of Summer Computer Simulation Conference, July 1976.

4. Townsend, G. E., Jr. (1963). *Orbital Flight Handbook*, Vol. 1, Part 1, NASA SP-33, NASA, Washington, D.C., 1963.

5. Bate, Roger D., Donald D. Mueller, and Jerry E. White (1971). *Fundamentals of Astrodynamics*, Dover Pubs, N.Y., 1971.

6. Reed, H. R. and Russell, C. M. (1964). *Ultra High Frequency Propagation*, Boston Technical Publishers, Inc. Lexington, MA, 1964.

7. Waters, J. W. (1992). "Submillimeter-Wavelength Heterodyne Spectroscopy and Remote Sensing of the Upper Atmosphere," IEEE Proc., November, 1992, p. 1679.

8. Kerr, D. 1965. *Propagation of Short Radio Waves*, Dover Publications, N.Y., N.Y., (1965). (Originally

published as Vol. 13 of the MIT Rad Laboratory Series, McGraw-Hill, 1951.)

9. Kamal, A. K. and Christopher, P. (1981). "Communications at Millimeter Wavelengths," Proc. ICC, June, 1981.

10. Frediani, D. J. (1979). "Technology Assessment for Future MILSATCOM Systems: The EHF Band," Lincoln Laboratory Project Report DCA-5, 12 April 1979.

11. Crane, R. K. (1980). "Prediction of Attenuation by Rain," IEEE Transactions on Communications, Vol. Com-28, No. 9, September 1980.

12. Ippolito, L. J., R. D. Kaul, and R. G. Wallace (1981). "Propagation Effects Handbook for Satellite Systems Design," NASA Reference Publication 1082 (Second Edition), December 1981.

13. Silver, S. (1965). *Microwave Antenna Theory and Design*, Dover, N.Y., 1965.

14. Lin, S. H. (1979). "Statistical Behavior of Rain Attenuation, Bell System Technical Journal, Vol. 52, No. 4, pp. 557-581.

15. Bean, B. R. and E. J. Dutton (1966). *Radio Meteorology*, NBS Monograph 92, U.S. Department of Commerce, 1966, pp. 270-274.

16. Wolfram, S. (1991). *MATHEMATICA a System for Doing Mathematics by Computer*, Second Edition, Addison Wesley Publishing Co., Inc., 1991.

Appendix: Total Loss in 1998, with I=10 Degrees

Figure A-1 shows expected total loss vs. TDRS-1 relay longitude and yaw for a Tidbinbilla ground station. Approximately 4 to 5 dB advantage is shown on the contour plot of Figure A-2 for a relay at 93E versus a relay at 85E.

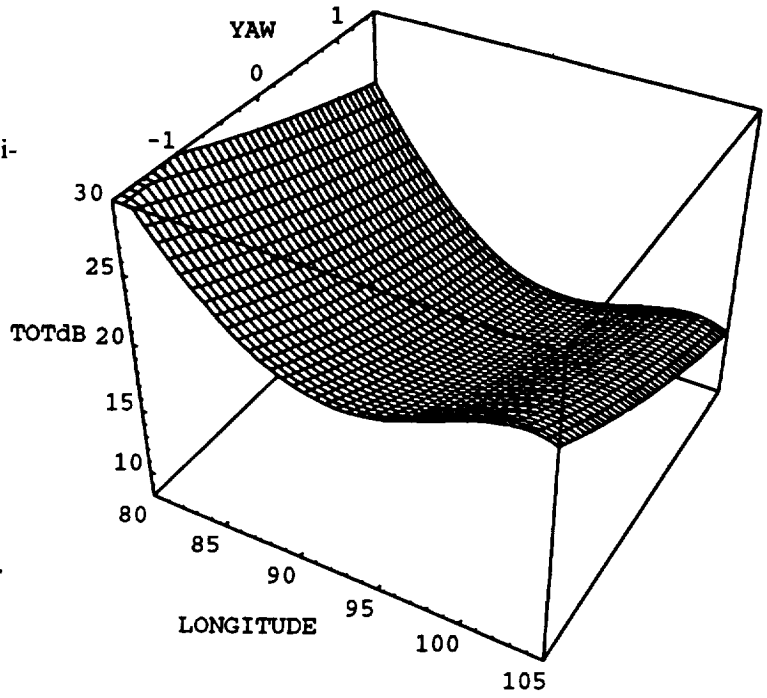

Figure A-1: Total Loss as a Function of Longitude and Yaw I=10,° August 1998

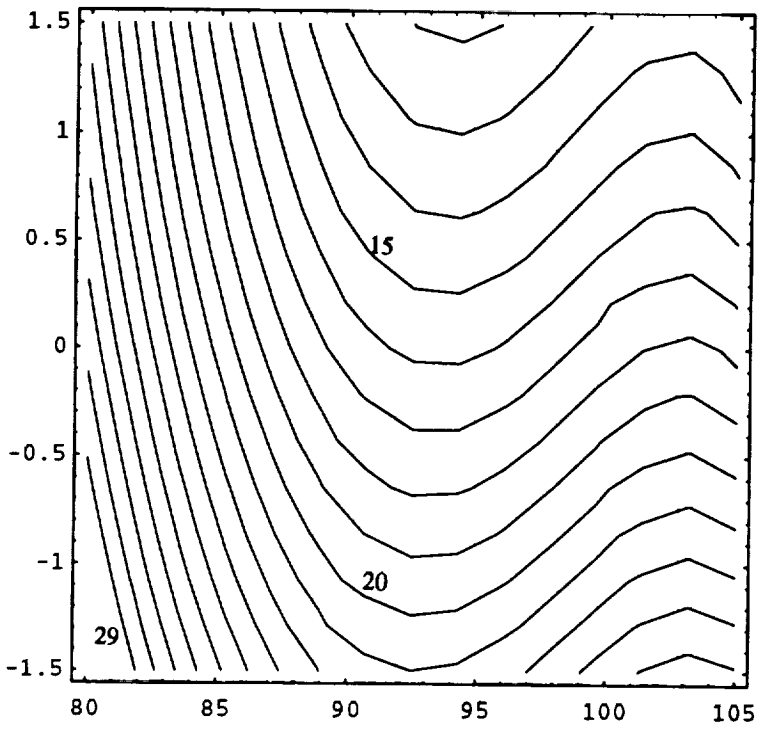

Figure A-2: Total Attenuation with 1 dB Contour Intervals I=10°, August 1998

MIS019B